Polymer Journal (2019) 51:283–294
https://doi.org/10.1038/s41428-018-0152-5

ORIGINAL ARTICLE

Effects of a special diluent as an agent of improving the crystallizability of poly(L-lactic acid)

Pham Thi Ngoc Diep[1] · Masatsugu Mochizuki[2] · Mikio Doi[2] · Hideaki Takagi[3] · Nobutaka Shimizu[3] · Noriyuki Igarashi[3] · Sono Sasaki[1] · Shinichi Sakurai[1]

Received: 2 August 2018 / Revised: 21 September 2018 / Accepted: 15 October 2018 / Published online: 21 November 2018

Abstract

It has been found that a special type of diluent can act as an agent to improve the crystallizability of poly(L-lactide) (PLLA). To present clear experimental results to support such an ability, we used time-resolved small and wide-angle X-ray scattering (SWAXS) to follow the isothermal crystallization of PLLA. The WAXS results show the enhancing effects of the diluent on the crystallization of PLLA, such as the reduction of the induction period and the acceleration of crystallization. Furthermore, the transformation from the δ phase to the α phase was also detected in the presence of the diluent. The growth of the crystalline lamellae in their thickness direction was accelerated in the presence of the diluent. It was further found that the diluent can accelerate the space filling of the stacks of crystalline lamellae in the specimen.

Introduction

In the past several tens of years, the environmental problems and depletion of fuel resources have strongly influenced science and technology, especially materials science. Scientists deeply consider materials that are independent from petroleum and are less harmful to the environment. Therefore, biobased materials are the most promising candidates as new materials for the future. Several biodegradable polyesters have been developed, such as poly(lactic acid) (PLA), polyhydroxyalkanoate, poly(caprolactone), poly(butylene succinate), and so on [1–3]. Among them, PLA has received much attention because PLA is a polymer that is biodegradable and made of biobased materials. PLA has asymmetric carbons and contains the two enantiomers poly (L-lactic acid) (PLLA) and poly (D-lactic acid) (PDLA), which are both crystalline. There are three crystalline forms of PLLA (α, β, and γ forms) due to the preparation method. The most common polymorph is the α form, which can be formed through melt crystallization or by crystallization from solution. X-ray diffraction has revealed that the α form is a pseudo-orthorhombic system, composed of two chains with a 10/3 helical conformation. Its lattice parameters are $a = 1.07$ nm, $b = 0.645$ nm, and $c = 2.78$ nm [4, 5]. The β form is obtained under high drawing and high temperature conditions, forming an orthorhombic crystal that consists of chains with a 3/1 helical conformation. The lattice parameters are $a = 1.031$ nm, $b = 1.821$ nm, and $c = 0.90$ nm [6]. For the third form (the γ form), Cartier et al. [7] reported that it grew epitaxially on hexamethylbenzene. Two antiparallel helices are packed in one-orthorhombic unit cell with lattice parameters $a = 0.995$ nm, $b = 0.625$ nm, and $c = 0.88$ nm. Subsequently, Zhang et al. [8, 9] also reported a disordered α' form (δ form) that is lower density and can transform to the α form by heating [10].

Although PLLA is an ecofriendly material, the application of PLLA has been rather limited until now due to its relatively poor thermal stability, poor long-term durability, lower impact strength, and poor crystallization abilities. Several approaches have been made to improve the poor properties of PLLA. Blending PLLA and PDLA or constructing a block copolymer comprising PLLA and PDLA block components are

Electronic supplementary material The online version of this article (https://doi.org/10.1038/s41428-018-0152-5) contains supplementary material, which is available to authorized users.

✉ Shinichi Sakurai
shin@kit.ac.jp

[1] Department of Biobased Materials Science, Kyoto Institute of Technology, Matsugasaki, Sakyo-ku, Kyoto 606-8585, Japan

[2] Taiyo Kagaku Co., Ltd, Mie, Japan

[3] High Energy Accelerator Research Organization (KEK), Tsukuba, Japan

popular methods to utilize the stereocomplexation [11–17]. During polymer processing, the polymer will be melted at high temperature and then quickly cooled to the desired temperature with as rapid a cooling rate as possible (a cooling rate of approximately (approx.) 1000 °C/min). However, due to the very fast cooling rate, PLLA has many drawbacks in terms of its crystallization. These are due to the low crystallization rate and the long induction period. Namely, PLLA requires a longer time to complete its crystallization process. According to the time limitation of polymer processing, the products continue the slow crystallization process, even at room temperature, after polymer processing. This means that the product structure gradually changes and that the final product is shrunken. To overcome this drawback, many researchers have aimed to improve the crystallizability (acceleration of crystallization and shortening of the induction period) of PLLA [18, 19]. As a matter of fact, by adding a nucleation agent, the requirements will be met. In principle, nucleation agents work in the solid state. Although the liquid-type additive that plays the role of a diluent (plasticizer) is considered to decrease polymer crystallizabilities, it has been found that a special diluent can enhance the crystallizability of PLLA [20]. Therefore, the purpose of this work is to present clear experimental results to support the positive effects of the diluent (organic acid mono glyceride (OMG)) on the crystallization of PLLA. For this purpose, simultaneous small and wide-angle X-ray scattering (SWAXS) were used to follow the isothermal crystallization of PLLA. Differential scanning calorimetry (DSC) was also used for the same purpose.

Experimental section

Specimens

We used two types of PLLA samples that were purchased from NatureWorks LLC with 1.4% D-content (PLLA4032D) and 0.5% D-content (PLLA2500HP). The information for these samples and code names of the specimens are listed in Table 1.

The MFR test was conducted at 210 °C with the standard weight of 2.16 kg. The diluent that was used was a type of OMG which contains an organic acid as a succinic acid and a saturated fatty acid as a stearic acid. OMG is a product of Taiyo Kagaku Co., Ltd. The commercial name of OMG is Chirabazol D, which is a biobased material. The OMG has a molecular weight of 500 and a melting temperature of T_m = 67 °C.

Polarizing optical microscope (POM)

The sheet specimen (thickness of approx. 250 μm) was cut into a small piece with a size of 2 mm × 2 mm. Then, it was placed between two pieces of cover glass (thickness of 0.12 mm). The specimen was heated from room temperature (RT) to 200 °C, isothermally maintained at 200 °C for 5 min, and cooled to the crystallization temperature of 110 °C at a cooling rate of 20 °C/min under a liquid nitrogen flow.

Table 1 Sample name

Sample	D-content	MFR (melt flow rate) (g/10 min at the load of 2.16 kgf, 210 °C)
PLLA4032D	1.4%	7.0
PLLA2500HP	0.5%	8.0
Code Name	Description	Concentration of OMG
D1.4	PLLA4032D	–
D1.4/OMG	PLLA4032D/OMG	1 wt%
D0.5	PLLA2500HP	–
D0.5/OMG	PLLA2500HP/OMG	1 wt%

Kinetics of crystallization as analyzed by DSC

The sheet specimen was cut into small pieces with weights of approximately 4–6 mg. The Al pan (Standard Pan; serial number: 900786.901) and the lid (Standard Lid; serial number: 900779.901) used in this measurement were purchased from TA Instrument, Inc. (New Castle, Delaware, USA) or TA Instruments Japan K.K. (Tokyo, Japan). The specimen was placed in the pan, covered with the lid, and then sealed with a crimper. The sealed Al pan was set in the DSC furnace, and the measurements were performed using the DSC Universal V3.9 A (TA Instruments). The detailed measurement conditions are given in the Results and discussion section.

Crystallization kinetics as analyzed by SWAXS

Figure 1 shows the experimental setup of the SWAXS measurements for isothermal crystallization. The sheet specimen was cut into a small piece with a circular shape with a diameter of 4 mm. Then, 3–4 layers of the specimens were stacked in the Al sample cell, which had a thickness of 1 mm and a diameter of 4 mm. Thus, we attempted to completely fill the space of the sample cell with the stacked specimens, with the total thickness being nearly 1 mm. The stacked specimens were sandwiched between 2 pieces of the Kapton film (thickness: 25 μm, DuPont–Toray Co., Ltd. Japan), and the sample cell was sealed. A thermosensor (K type) was inserted directly into the specimen to measure the exact specimen temperature.

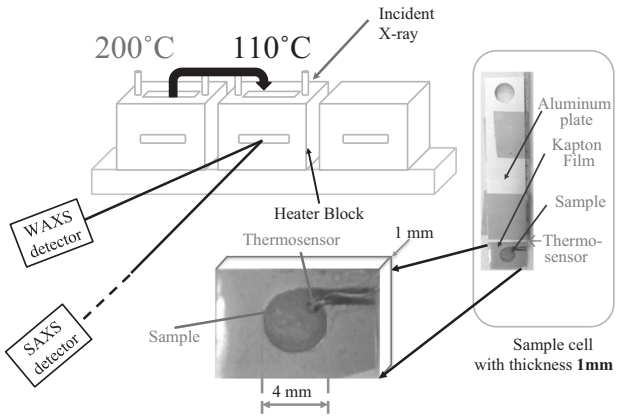

Fig. 1 Schematic representation of the experimental setup for isothermal crystallization by SWAXS

First, the specimen was heated to 200 °C from RT. When the temperature of the specimen reached 200 °C, the specimen was isothermally maintained at that temperature for approximately 10 min to allow the specimen to melt completely. Afterward, the sample cell was quickly moved to another heater block where the temperature was maintained at 110 °C, and then time-resolved measurements of SWAXS were initiated. The SWAXS measurements were conducted for the specimen during isothermal crystallization with an exposure time of 5 s using PILATUS 100 K for WAXS and PILATUS 1 M for SAXS (DECTRIS Ltd., Baden, Switzerland) as a two-dimensional detector at BL-6A of the Photon Factory in High Energy Accelerator Research Organization, Tsukuba, Japan. The sample-to-WAXS and -SAXS detector distances were 40 mm and 2 m, respectively, and the X-ray wavelength was 0.150 nm. The details of the SAXS beamline of BL-6A are reported elsewhere [21].

Results and discussion

POM results

Figure 2 shows the POM images of two representative specimens obtained at 110 °C. Figure 2a, b shows D0.5 at 1000 s and Fig. 2c, d shows D0.5/OMG at 200 s. The images in Fig. 2a, c are expanded views of the regions specified with yellow rectangles in Fig. 2b, d, respectively. Figure 2b shows an almost full view of the POM field, and it is apparent that almost 100% of the specimen space was filled with the spherulites. This is reasonable compared to the other results of DSC, WAXS, and SAXS that show the final stage of the crystallization at 1000 s. In Fig. 2d, it is apparent that there is still open space even at 200 s, for which the other results ensure the final stage. However, Fig. 2d does not show the full field. In the supporting information, the full-field POM image is shown in Figure S1, which clearly shows nearly 100% coverage of the specimen space by spherulites.

The POM image of specimen D0.5 shows a regular spherulite. The spherulite seemed to be regularly formed from the onset of its formation, as the clear Maltese cross can be seen. On the other hand, the spherulite of specimen D0.5/OMG shows an irregular feature near its center. This phenomenon may be related to the accelerated crystallization due to OMG. Namely, some of the crystallites grow quickly by forming a needle-like shape instead of a two-dimensional disk-like (ribbon) shape. Although it is difficult to clearly observe such small needle-like crystallites in the early stage by POM, the irregular feature near the center of the spherulite for the specimens with OMG implies that some of the crystallites form needle-like shapes and, in turn, that the regular growth of ribbons (i.e., lamellar crystallites) may be disturbed.

Kinetics of crystallization as analyzed by DSC

DSC curves measured in the heating process

DSC measurements were performed for 4 specimens with 2 heating runs and 1 cooling run at the rate of 10 °C/min. The DSC curve of the second heating run was used to clarify the glass transition (T_g), cold crystallization (T_{cc}) and melting (T_m) temperatures. Here, the first heating run was performed up to 200 °C, and then the specimen was cooled to RT. Figure 3a, b shows the DSC curves (second heating run) with the values of T_g, T_c, and T_m.

From both figures, the results clearly show that the specimens with OMG have a lower T_g than the neat PLLA specimens. This supports the effect of OMG as a diluent. Additionally, the T_g values for D0.5 and D0.5/OMG are slightly lower than those for D1.4 and D1.4/OMG. This is due to the slight difference in molecular weights of the PLLA samples (D0.5 and D1.4).

On the other hand, the T_{cc} values for D0.5 and D0.5/OMG are much lower than those for D1.4 and D1.4/OMG. This clearly indicates the higher crystallization ability of the specimens with the lower D-content. Furthermore, T_m values are higher for D0.5 and D0.5/OMG specimens than for D1.4 and D1.4/OMG. This implies that the crystallites were thicker in the D0.5 and D0.5/OMG specimens, again indicating the superiority of crystallization of the specimens with the lower D-content. For the effects of adding OMG, there was a trivial difference between the D1.4 and D1.4/OMG specimens in T_{cc} and T_m. In contrast, T_{cc} was much lower for the D0.5/OMG specimens compared to the neat D0.5 specimen. This suggests the improved crystallization ability through the addition of OMG, although the OMG

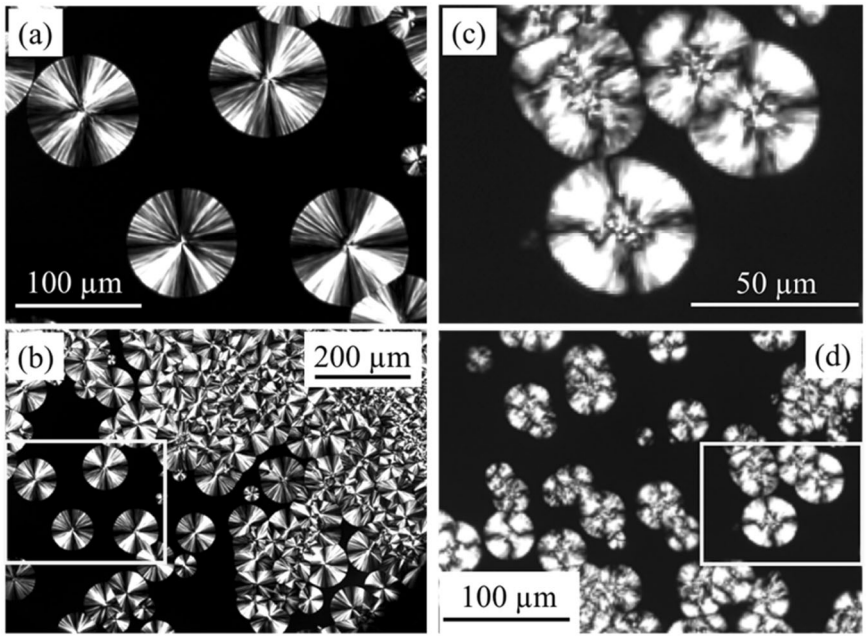

Fig. 2 POM images of specimens obtained at 110 °C. **a**, **b** D0.5 at 1000 s, and **c**, **d** D0.5/OMG at 200 s. The images in (**a**) and (**c**) are expanded views of the regions specified with yellow rectangles in (**b**) and (**d**), respectively

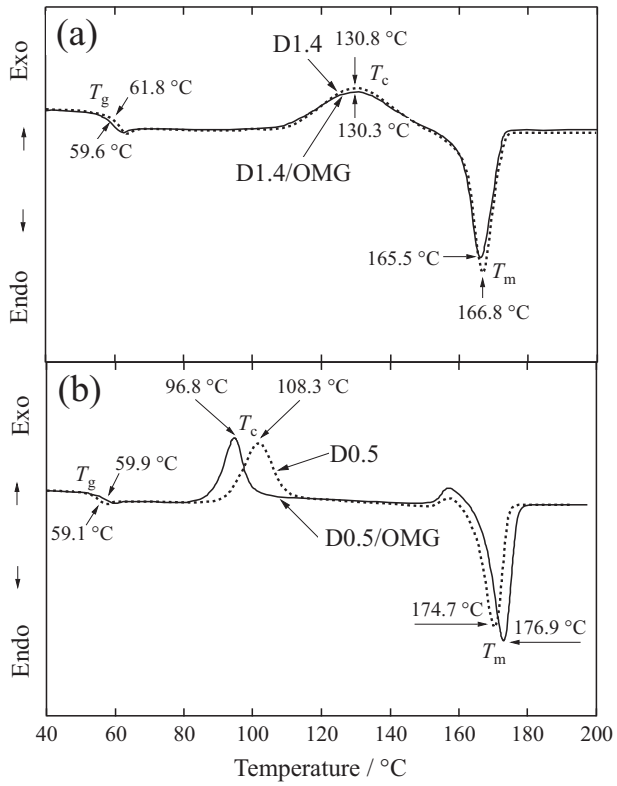

Fig. 3 **a** Second heating run DSC curves of specimens D1.4 and D1.4/OMG. **b** Second heating run DSC curves of specimens D0.5 and D0.5/OMG

amount was as low as 1%. Finally, it is notable to observe the exothermic peaks around 160 to 165 °C in Fig. 3b. This result indicates the crystal transition (from the δ form to the α form). In contrast, no such peak was observed in Fig. 3a.

Isothermal crystallization by DSC

The specimens were heated from RT to 200 °C at a heating rate of 10 °C/min and were then isothermally maintained at 200 °C for 2 min to erase the thermal history of the specimen. Subsequently, the specimen was quickly cooled to the crystallization temperature (110 °C) at a cooling rate in the range of 15–40 °C/min.

When the temperature reached 110 °C, an isothermal crystallization measurement was performed. Upon isothermal crystallization, the evolution of the exotherm ($\Delta H_c(t)$) was measured as a function of time. By integration of the exotherm, the temporal evolution of the crystallinity, $\phi(t)$, was evaluated by

$$\phi(t) = \frac{\int_{t=0}^{t} \Delta H_c(t)dt}{\Delta H_m^0}, \quad (1)$$

where ΔH_m^o is the enthalpy of fusion of the 100% crystal of PLLA. Righetti et al. [22] reported that the ΔH_m^o values of the δ and α forms are 107 and 143 J/g, respectively. PLLA crystals exist mostly in the δ form at a low temperature of 110 °C. Figure 10 shows that our specimens have the α form, of which the amount is quite small (less than 3%). Thus, the value of ΔH_m^o is 107 J/g. The plots of the crystallinity $\phi(t)$ as a function of time are shown in Fig. 4. The initial slope of the plot is in the following order:

$$\text{slope(D1.4)} < \text{slope(D1.4/OMG)} < \text{slope(D0.5)} < \text{slope(D0.5/OMG)}$$

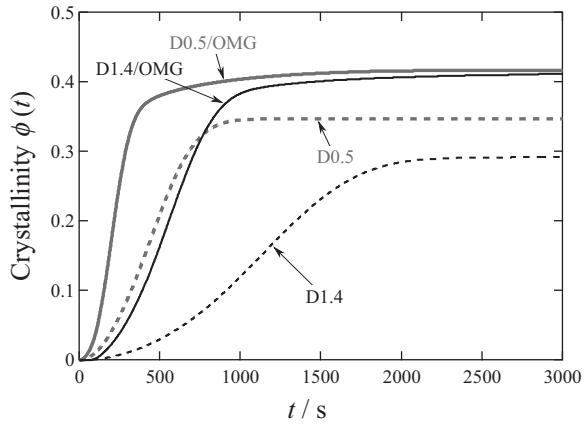

Fig. 4 Temporal evolution of crystallinity as a function of time by DSC

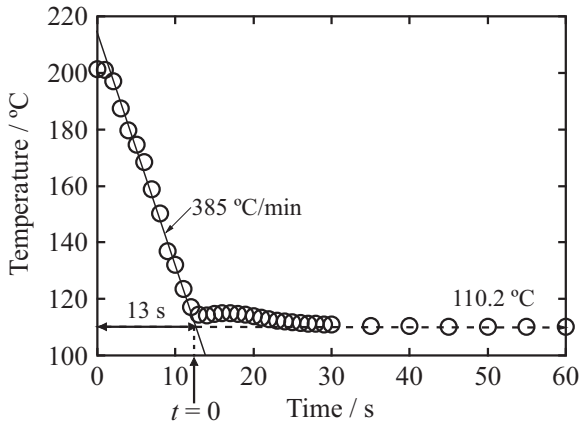

Fig. 5 Temperature changes after a T-jump from 200 °C to 110 °C

It is suggested that the crystallization rate increases as the D-content decreases, as well as with the addition of OMG. From the crystallinity results, not only the slope (the crystallization rate) but also the final values of the crystallinity indicate the significance of the addition of OMG, since the final crystallinity increased from 0.292 to 0.411 for the D1.4 specimen and from 0.347 to 0.417 for the D0.5 specimen after the addition of OMG.

Crystallization kinetics as analyzed by SWAXS measurements

Temperature changes upon T-jump from 200 °C to 110 °C

The specimen was heated to its melt state (200 °C) and cooled to its crystallization temperature (110 °C) at a very high cooling rate. An approximately 1000 °C/min rate is requested from the perspective of the polymer processing condition.

Our experimental condition enabled a cooling rate as high as 385 °C/min, as shown in Fig. 5. Although this is still lower than the rate required for industrial processing, this condition was our best attempt. From the plot in Fig. 5, the zero crystallization time was determined as the crossing point of an approximated line of the cooling process and a horizontal line of a stabilized temperature at 110.2 °C. The temperature was equilibrated at a time of 13 s.

WAXS results from the SWAXS measurements

Figure 6 shows the changes in the one-dimensional WAXS (1d-WAXS) profiles for D1.4 and D1.4/OMG. These profiles were obtained by conducting a sector average. Here, q denotes the magnitude of the scattering vector as defined by $q = (4\pi / \lambda) \sin(\theta/2)$ with λ and θ being the wavelength of the X-ray and the scattering angle, respectively. In the early stage, the 1d-WAXS profile shows a 100% amorphous halo. As time progresses, a small crystalline peak appeared and grew. The number of crystalline peaks also increased. A peak decomposition was conducted to separate the crystalline peaks from the amorphous halo peak. From the values of the decomposed peak area, the apparent degree of crystallinity was evaluated using

$$\phi(t) = \frac{\sum A_c}{\sum A_c + A_a}, \quad (2)$$

where $\sum A_c$ is the summation of the peak area of the crystalline peaks and A_a is the peak area for the amorphous halo. The apparent crystallinity is plotted as a function of the crystallization time in Fig. 7a for all specimens. Note here that the data points with an interval of 5 s are connected with lines. The same approach for displaying the data is used for SWAXS data in the following figures. By comparing the results shown in Figs. 4 and 7a, similar values can be recognized except for the D0.5/OMG specimen. In general, the crystallinity based on the WAXS results is not identical to that based on the DSC results. The latter is closer to the real value of the crystallinity. On the other hand, the former, based on the WAXS results, is apparent because the WAXS profile only cover a limited q range.

The overall shapes of the apparent crystallinity are similar to those shown in Fig. 4, but the details are somewhat different. Figure 7b shows the apparent crystallinity plots in the early stage. Line fitting was conducted to approximate the tendency in the very early stage of the crystallization process. Then, the effect of the OMG is very clear for the acceleration of crystallization. The slope of specimen D1.4/OMG is 1.6 times higher than that of the neat D1.4. In addition, the slope of specimen D0.5/OMG is 3.5 times higher than that of the neat D0.5. This clearly indicates the higher crystallization rate of the specimens in the presence of OMG. Furthermore, the slopes of the

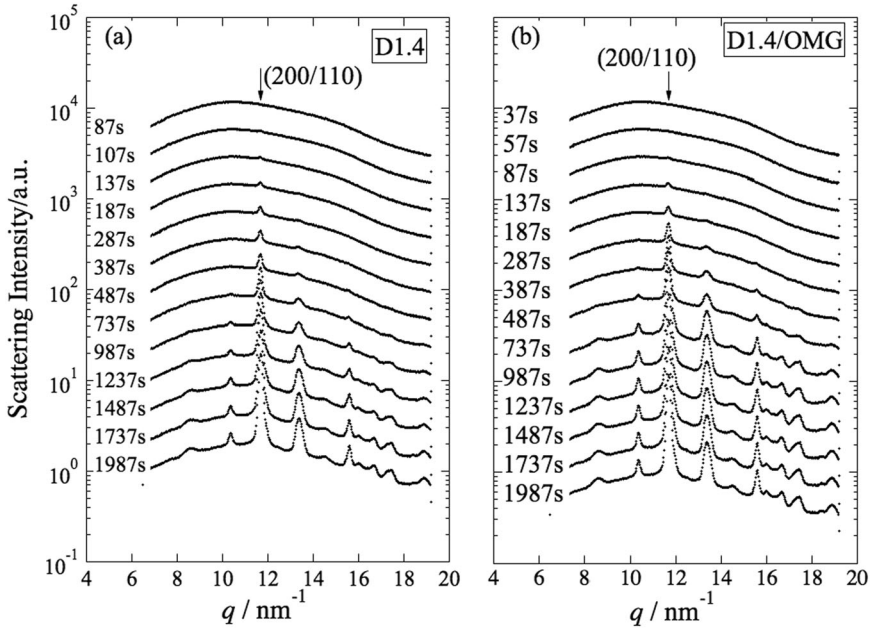

Fig. 6 The 1d-WAXS profiles for samples D1.4 and D1.4/OMG

apparent crystallinity plots are higher for specimens D0.5 and D0.5/OMG than those for specimens D1.4 and D1.4/OMG. This clearly indicates that the lower D-content specimens have higher crystallization abilities.

Furthermore, the induction period was evaluated from the plots in Fig. 7b, and the evaluated induction period is summarized in Table 2. From the results of the induction period, the effect of OMG is again confirmed as the reduction of the induction period. Additionally, the specimens with a lower D-content have an obviously shorter induction period than the specimens with a higher D-content.

Avrami analyses were performed to distinguish the crystallization kinetics for all specimens and clarify the effects of adding OMG. It is well known that the evolution of the crystallinity is proceeded by the Avrami function [23, 24] as:

$$\phi(t) = \{1 - \exp[-(kt)^n]\} \times \phi^{\infty}, \quad (3)$$

where k is the rate coefficient and n is the Avrami exponent relevant to the dimensionality of the crystallite growth. The Avrami plots for the WAXS results are shown in Fig. 8, where t_0 denotes the induction period. Overall, the crossover of the crystallization kinetics is discernible for all specimens. However, the crossover time is very different depending on the specimen. In the early stage, a smaller slope of 1.05 to 2.10 was observed, whereas a larger slope of 1.79 to 2.92 was observed in the later stage. It was found that the early-stage slope was sensitively changed by the value of t_0 (the induction period). Therefore, we do not discuss the effects of OMG in the early stage. On the other

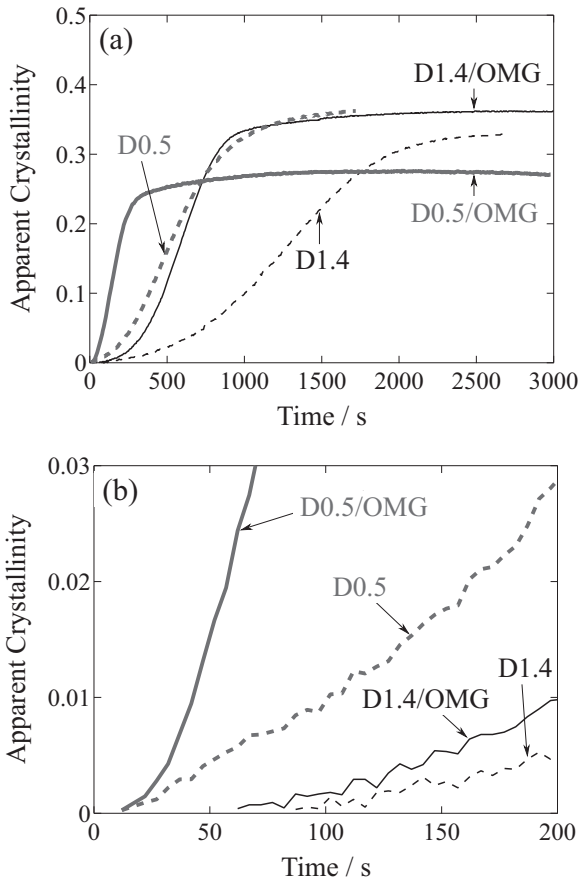

Fig. 7 **a** Apparent crystallinity as a function of time (overall) and **b** in the early stage (less than 200 s). Note here that the data points within an interval of 5 s are connected with lines. A similar approach to data display is applied for SWAXS data in the following figures

Table 2 Induction period

Samples	without OMG	with OMG (1 wt%)
D1.4	89.5 s	64.5 s
D0.5	14.5 s	9.5 s

hand, in the later stage beyond the crossover time, the slope hardly changed with the values of t_0. It is clear that the slope decreased dramatically with the addition of OMG for D0.5. This indicates that the growth dimensionality of the crystallites decreased. Since it is possible to detect the wide distribution of the spherulite size in Fig. 2b, d, homogeneous nucleation [23] can be assumed. Therefore, the dimensionality of crystallite growth can be evaluated as $(n-1)$ (about one-dimensional growth) from the value of the Avrami exponent n. Unfortunately, it was not possible to detect the formation of needle-like crystallites by POM in the later stage of crystallization for the D0.5/OMG specimen. The POM always indicated spherulite formation. The reason for the discrepancy between the WAXS Avrami analyses and the POM observation is not clear at present. In contrast, there is no apparent effect of the addition of OMG on the slope in the later stage for D1.4. It is also notable that the addition of OMG is more effective for D0.5 than D1.4, as detected in the effects on T_{cc} (Fig. 3) and on the crystallization rate (Fig. 7b). Another notable effect is observed in the crossover time. Namely, through the addition of OMG, the crossover time decreases significantly. Once again, the extent of the reduction is much larger for D0.5 than D1.4.

The d spacing for the main reflection peak (200/110) is shown in Fig. 9. As time proceeds, the d spacing decreased, especially for the specimens of D0.5 and D0.5/OMG, which implies increasing density as a function of crystallization time. Moreover, on the 1d-WAXS profile, there is a small shoulder adjacent to the main reflection peak (200/110) in Fig. 10. This suggests the appearance of another peak in this q range. The computational peak decomposition was conducted in this q range as shown in Fig. 10 to separate the shoulder. Since the q position of the shoulder is higher than the main peak, the d spacing of the plane that produces the shoulder reflection is shorter, which in turn indicates a higher density. Therefore, the main peak can be ascribed to the lower density phase, which is the δ phase (α' phase), whereas the shoulder reflection is ascribed to the higher density phase, which is the α phase. According to Zhang et al. [9], the contribution from the α phase should be observed around the 203 reflection ($q = 13.3\ \mathrm{nm}^{-1}$) and 210 reflection ($q = 15.6\ \mathrm{nm}^{-1}$). However, no such side peak appeared. This implies that the appearance of the side peak near the 200/110 reflection (Fig. 10) may be a false peak. However, we can see a clear difference in the appearance (the peak area) of the side peak as a function of time for three different specimens, as shown in Fig. 11. Therefore, we are confident that the side peak is real.

Figure 11 shows the α phase peak area as a function of time. The appearance of the α phase was not detected for the D1.4 specimen. By adding OMG, the area of the peak for the α phase increased from 700 s for the D1.4/OMG specimen. On the other hand, in the case of specimen D0.5, the α phase peak appeared from 500 s but then leveled off. For specimen D0.5/OMG, the appearance of the α phase occurred in an earlier stage, approximately 300 s. However, the α phase is detected but with the small amount (α phase fraction is less than 3%). When the α phase increased very much, this may degrade the impact strength [25]. Fortunately, the δ phase in case of OMG addition is still large enough to maintain the better mechanical properties of the PLLA.

SAXS results from the SWAXS measurements

SAXS profiles for the D1.4 and D1.4/OMG specimens are shown in Fig. 12. Figure 12c, d shows the corresponding Lorentz-corrected profiles ($q^2\ I(q)$ vs. q). As clearly shown in Fig. 12a, b, the scattering contains strong contributions from foreign particles. Therefore, the scattering intensity of the molten state including the contribution of the foreign particles should be subtracted from all of the other SAXS profiles [26, 27]. However, without subtraction, the Lorentz-corrected profiles appear to have an almost negligible contribution from the scattering intensity at the molten state. Therefore, we did not conduct subtraction of the molten state scattering profile for further analyses.

The evolution of a peak is clearly observed. To evaluate the crystalline lamellar thickness L and the long period D, the correlation function $\gamma(r)$ was calculated from the 1d-SAXS profile through the following equation (inverse Fourier transform method).

$$\gamma(r) = \frac{\int_0^\infty I(q) q^2 \cos(qr) dq}{\int_0^\infty I(q) q^2 dq}. \quad (4)$$

Extrapolation of the scattering intensity $I(q)$ in small-q and large-q regions [28] is required to calculate the correlation function. In general, the extrapolation of the scattering intensity $I(q)$ in a small-q region is based on the Guinier's law, $I(q) \sim [\exp(-kq^2)]$. In a large-q region, the extrapolation is based on the Porod's law, $I(q) \sim q^4$, which is shown in Fig. 13a. Here, the black curve is an experimentally obtained profile combined with the Guinier and Porod extrapolations.

By conducting Guinier and Porod extrapolations for the scattering profile in both small-q and large-q regions, we obtain a smooth and continuous 1d-SAXS profile over the

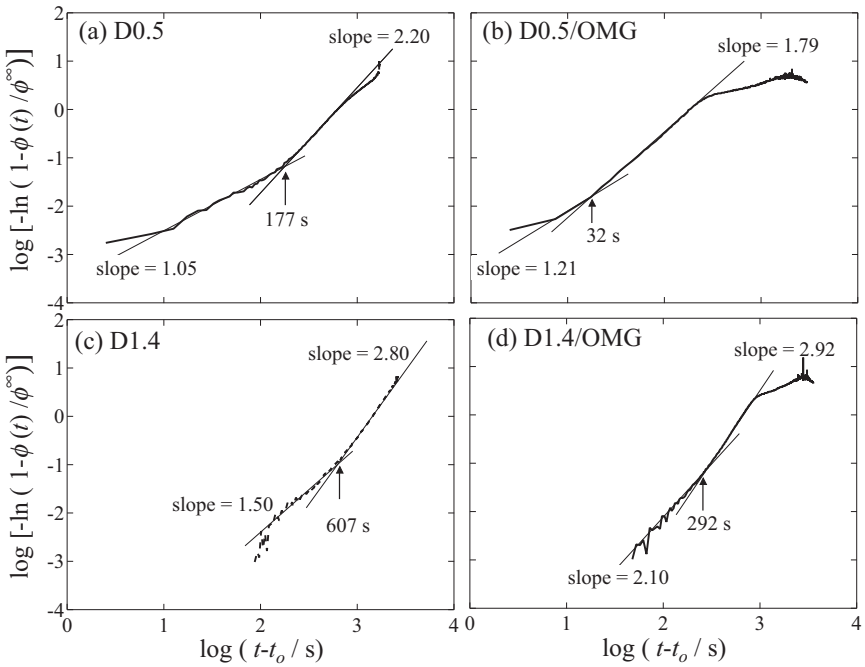

Fig. 8 Avrami plots based on the WAXS results for **a** D0.5, **b** D0.5/OMG, **c** D1.4, and **d** D1.4/OMG specimens

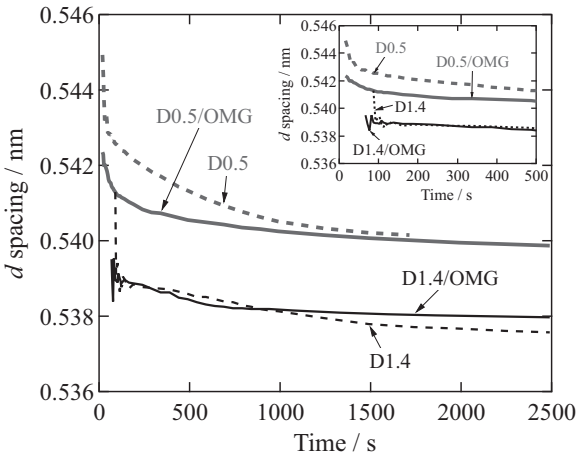

Fig. 9 The *d* spacing for the main reflection peak (200/110) as a function of time

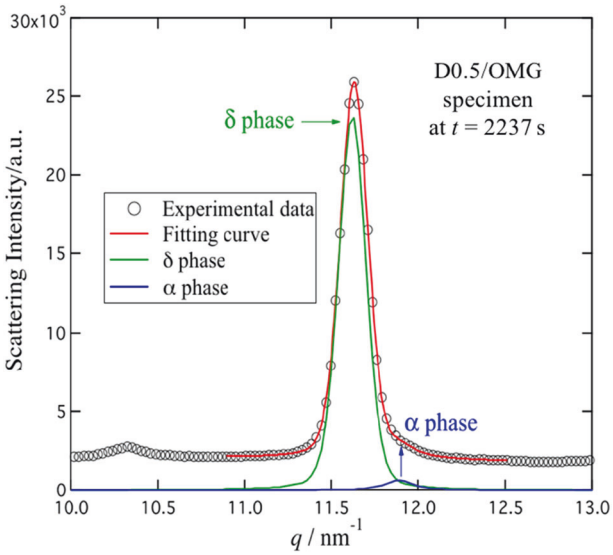

Fig. 10 WAXS profile of D0.5/OMG at $t = 2237$ s in the q range of 10–13 nm^{-1} to highlight the existence of the shoulder peak around $q \approx 11.85\ nm^{-1}$ and the decomposed peaks for the main peak (the δ phase) and the shoulder peak (the α phase)

full range of q. However, such extrapolations for every SAXS profile over the course of isothermal crystallization consume a lot of time. For the sake of reducing the analyses for a large amount of data, we prefer to omit this extrapolation procedure. To do so, we compared the correlation function derived from the SAXS profile itself and that from the extrapolated combination profile. Figure 14b compares the correlation functions obtained with the two different types of data analyses. The curves are very similar and give similar values of D and L. Thus, we ensured the validity of the correlation function that was directly calculated from the SAXS profile with no extrapolation in small-q and large-q regions.

According to Strobl [24], based on the two-phase model with crystalline and amorphous phases, the thickness of the thinner phase can be evaluated from the plot of $\gamma(r)$ in Fig. 13b at the crossing point of the horizontal line, which passes through the minimum point of $\gamma(r)$, and the approximated line of $\gamma(r)$ in the small r range. In the case of an early stage of isothermal crystallization, the obtained value can be considered as the lamellar thickness (L)

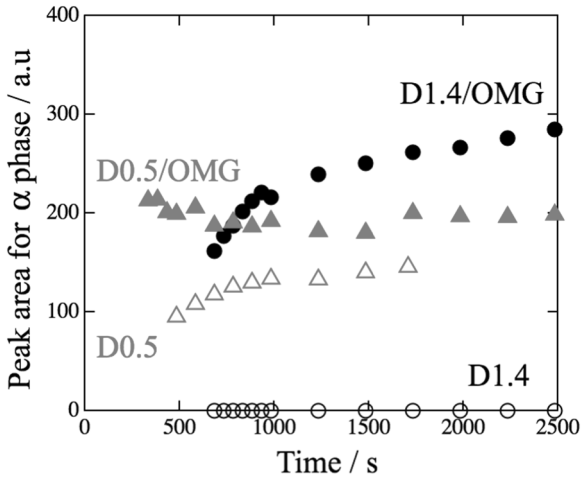

Fig. 11 Peak area for the α phase as a function of time

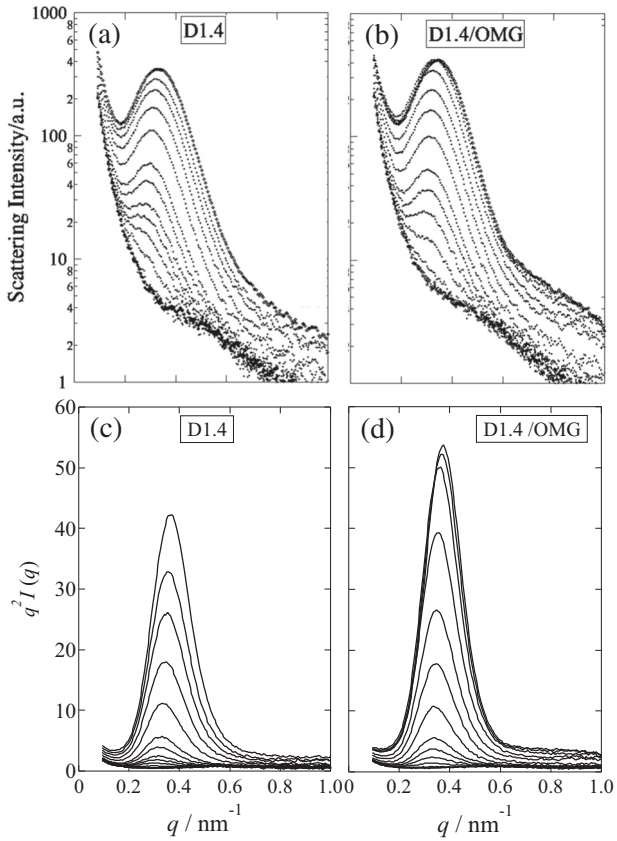

Fig. 12 The 1d-SAXS profiles for **a** D1.4 and **b** D1.4/OMG upon isothermal crystallization at 110 °C from 12 to 1987 s. The (**c**) and (**d**) are the corresponding Lorentz-corrected profiles

because the lamellar phase is thinner than the amorphous phase.

Figure 14 shows changes in the lamellar thickness as a function of time. As time proceeded, the lamellar thickness increased in the early stage and then leveled off in the later stage. The rate of increase of the lamellar thickness in the

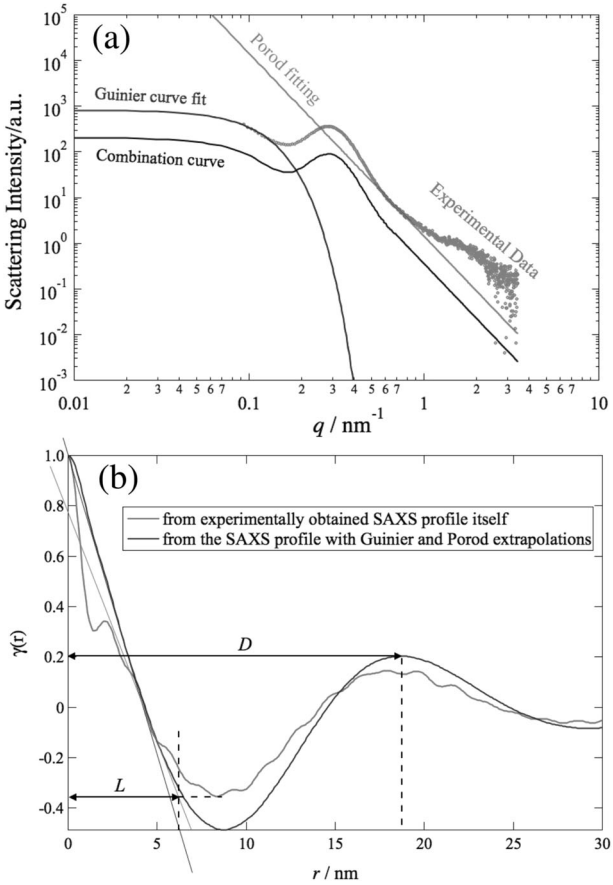

Fig. 13 **a** Guinier and Porod extrapolations for the experimentally obtained scattering profile. **b** Correlation functions obtained with two different types of data analyses

early stage is in the following order:

$$\text{slope(D1.4)} < \text{slope(D1.4/OMG)} < \text{slope(D0.5)} < \text{slope(D0.5/OMG)}.$$

These results suggest that the lamellar thickness increased quickly in the early stage of crystallization due to a decrease in the *D*-content and the addition of OMG. Specimen D0.5/OMG experienced a termination of lamellar growth very early (at 300 s) instead of continuous growth, as experienced by the other specimens (D1.4, D1.4/OMG, and D0.5). The ultimate lamellar thicknesses (at 3000 s) for all specimens are relatively similar, although the value for the D0.5/OMG is 0.94 times those of the others.

It is interesting to note that the overshoot phenomena of the growth in lamellar thicknesses are discernible for all specimens in Fig. 14 (it is also more or less even for the D1.4 neat specimen). Namely, the lamellar thickness reached a maximum and then decreased due to further annealing. The overshoot may be explained as follows. Less dense crystallites may be formed in the early stage, as

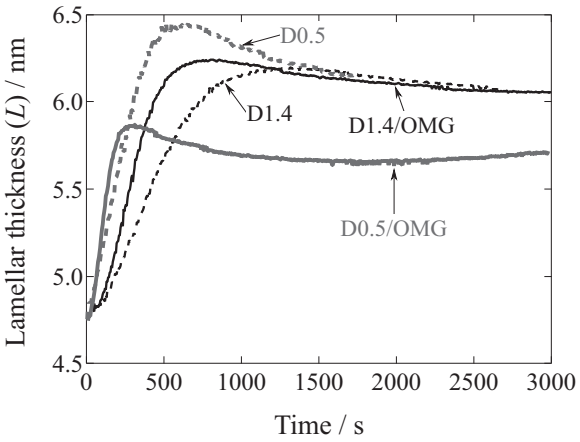

Fig. 14 Lamellar thickness L as a function of time

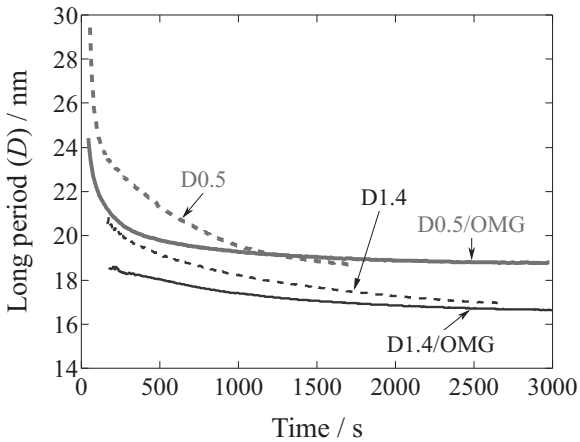

Fig. 15 Long period D as a function of time

shown in Fig. 9. Although L increased due to forwarded crystallization, densification of the less dense crystallites occurred. This process results in a decrease in L. Thus, counter effects occur concurrently, and therefore the overshoot can be explained. Due to the quick crystallization of the D0.5 and D0.5/OMG specimens, the overshooting of L is pronounced.

From the correlation function, the long period D was also evaluated and is shown in Fig. 15. The long period decreases mainly due to the decrease in the amorphous layer; a part of the amorphous layer is reordered in a higher-order structure and contributes to the development of thicker lamellae. Therefore, it is more important to check the ratio of the lamellar thickness and the long period, which can be considered as the degree of crystallinity by assuming that the specimen is completely filled with stacks of lamellae with intervening amorphous layers.

$$\phi(t) = \frac{L}{D}. \tag{5}$$

The ratio L/D was calculated and is plotted in Fig. 16. Specimen D0.5/OMG shows the highest rate of increasing L/D in the early stage and earliest termination of growth of L/D. This behavior is similar to that of the crystallinity evaluation based on the WAXS results. Therefore, the reason for the earliest termination of the WAXS crystallinity for the D0.5/OMG specimen may be explained by the earliest termination of L/D behavior. Close examination of the behaviors of L and D gives the clue that L is lowest and D is largest at 3000 s for specimen D0.5/OMG. A comparison of Figs. 7a and 16 reveals that L/D is larger than the WAXS apparent crystallinity (ϕ) for all specimens in the early stage. This fact indicates that the lamellar stacks are sparsely distributed in the matrix of the amorphous phase in the early stage of crystallization.

Finally, we provide a plausible explanation for the effect of OMG in accelerating crystallization and reducing the induction period. Since T_g is lowered by the addition of OMG (in Fig. 3), it is considered that OMG is molecularly dispersed in the polymer. However, the total viscosity is not dramatically changed because only 1% is added. Even for this case, it would be considered that the OMG molecule can facilitate better folding of the polymer chains upon the formation of lamellar crystallites, as schematically illustrated in Fig. 17. Then, it is possible to decrease the surface free energy (σ_e) of the upper and lower planes of the crystallites, which are composed of chain folding. Figure 17 compares the free energy change upon the formation of the primary nucleus as a function of the thickness of the primary nucleus according to the Hoffman–Lauritzen theory for cases of larger and smaller σ_e; these correspond to poor regular folding and better regular folding with the aid of the diluent, respectively. Note here that these two curves only show a model case by changing the lamellar thickness by a constant lateral size. It is clear that the critical thickness is decreased ($l_2^* < l_1^*$), and therefore the induction period is reduced. Furthermore, the decreased energy barrier ($\Delta E_2^* < \Delta E_1^*$) and the higher curvature of the curve contribute to accelerating the crystallization. This can explain our experimental results. This further reminds us that a general diluent (plasticizer) can play a similar role as OMG when it is mixed in the polymer matrix as a very small aliquot (~1 wt%). We will report experimental results to confirm this hypothesis in a future publication.

Conclusion

We present experimental results to highlight the effect of OMG on the crystallization of PLLA by conducting DSC and simultaneous time-resolved SWAXS measurements

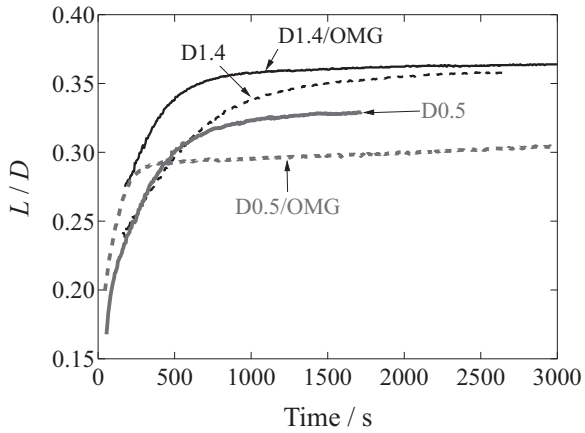

Fig. 16 Ratio of *L*/*D* as a function of time

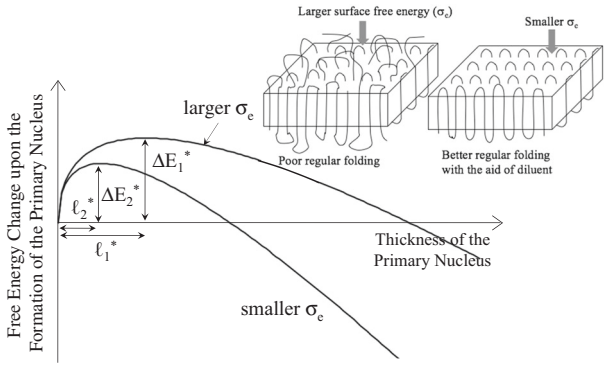

Fig. 17 Free energy change upon the formation of the primary nucleus as a function of the thickness of the primary nucleus according to the Hoffman–Lauritzen theory for cases of larger and smaller surface free energy (σ_e), which respectively correspond to poor regular folding and better regular folding with the aid of diluent

upon a T-jump from 200 to 110 °C. As a result of WAXS, it was found that the induction period was decreased after the addition of OMG. The crystallization rate in the early stage was enhanced significantly. The dimensionality of the crystallite growth, as revealed by the Avrami analyses, was dramatically decreased through the addition of OMG for sample D0.5, suggesting the formation of crystallites with needle-like shapes instead of two-dimensional disk-like shapes. The appearance of the denser α phase is noted. This suggests that the OMG can promote the formation of a more compact lattice structure.

The lamellar thickness and the long period were evaluated by SAXS analyses. By adding OMG, the growth rate of the lamellar thickness L increased significantly in the early stage of crystallization. The crystallinity results for specimen D0.5/OMG show the highest rate of increase in the early stage of the crystallization and the earliest termination of growth among the four specimens examined in this work. The earliest termination of the increasing crystallinity is characteristic of the D0.5/OMG specimen. Although the reason for this remains unclear, it may be considered that some of the crystallites of this specimen grew quickly by forming needle-like shapes instead of two-dimensional disk-like shapes. In fact, the irregular feature around the center of the spherulite was clearly observed by POM for the case of the D0.5/OMG specimen, which supports the disturbance of typical growth of the ribbon (the lamellar crystallite) in the early stage by the quick formation of needle-like crystallites.

Finally, we provide a plausible explanation for the effect of OMG on accelerating crystallization and reducing the induction period by considering better polymer chain folding with the aid of OMG. The model further reminds us that a general diluent (plasticizer) can play a similar role to OMG when it is mixed in the polymer matrix as a very small aliquot (~1 wt%). We will report experimental results to confirm this hypothesis in a future publication.

The effect of OMG on the Avrami exponent and the crystallization rate (Fig. 7) is much larger for sample D0.5 than sample D1.4. A plausible model for this effect of OMG, as shown in Fig. 17, will be important. If the OMG (diluent) can improve regular chain folding, this effect can be more pronounced for the higher L-content PLLA than for the lower L-content PLLA because the former is intrinsically capable of regular packing.

Compliance with ethical standards

Conflict of interest The authors declare no conflict of interest.

References

1. Garlotta D. A literature review of poly (lactic acid). J Polym Environ. 2001;9:63–84.
2. Kulkarni RK, Moore E, Hegyeli A, Leonard F. Biodegradable poly (lactic acid) polymers. J Biomed Mater Res A. 1971;5:169–81.
3. Martin O, Averous L. Poly (lactic acid): plasticization and properties of biodegradable multiphase systems. Polymer (Guildf). 2001;42:6209–19.
4. Sasaki S, Asakura T. Helix distortion and crystal structure of the α-form of poly (l-lactide). Macromolecules. 2003;36(no. 22):8385–90.
5. De Santis P, Kovacs AJ. Molecular conformation of poly(S-lactic acid). Biopolymers. 1968;6:299–306.
6. Hoogsteen W, Postema AR, Pennings AJ, Ten Brinke G, Zugenmaier P. Crystal structure, conformation and morphology of solution-spun poly (L-lactide) fibers. Macromolecules. 1990;23 (no. 2):634–42.
7. Cartier L, Okihara T, Ikada Y, Tsuji H, Puiggali J, Lotz B. Epitaxial crystallization and crystalline polymorphism of polylactides. Polymer (Guildf). 2000;41(no. 25):8909–19.
8. Zhang J, Tashiro K, Domb AJ, Tsuji H. Confirmation of disorder α form of poly (L-lactic acid) by the X-ray fiber pattern and polarized IR/Raman spectra measured for uniaxially-oriented samples. Macromol Symp. 2006; 242: 274-8.
9. Zhang J, Tashiro K, Tsuji H, Domb AJ. Disorder-to-order phase transition and multiple melting behavior of poly (L-lactide)

investigated by simultaneous measurements of WAXD and DSC. Macromolecules. 2008;41:1352–7.
10. Bremner T, Rudin A, Cook D. Melt flow index values and molecular weight distributions of commercial thermoplastics. J Appl Polym Sci. 1990;41:1617–27.
11. Hamad K, Kaseem M, Deri F. Preparation and characterization of binary and ternary blends with poly (lactic acid), polystyrene, and acrylonitrile-butadiene-styrene. J Biomater Nanobiotechnol. 2012;3:405.
12. Ikada Y, Jamshidi K, Tsuji H, Hyon SH. Stereocomplex formation between enantiomeric poly (lactides). Macromolecules. 1987;20: 904–6.
13. Pan P, Han L, Bao J, Xie Q, Shan G, Bao Y. Competitive stereocomplexation, homocrystallization, and polymorphic crystalline transition in poly (L-lactic acid)/poly (D-lactic acid) racemic blends: molecular weight effects. J Phys Chem B. 2015;119: 6462–70.
14. Tsuji H, Ikada Y. Stereocomplex formation between enantiomeric poly (lactic acid)s. XI. Mechanical properties and morphology of solution-cast films. Polymer. 1999;40: 6699–708.
15. Cao X, Mohamed A, Gordon S, Willett J, Sessa D. DSC study of biodegradable poly (lactic acid) and poly (hydroxy ester ether) blends. Thermochim Acta. 2003;406:115–27.
16. Tien N-D, Sasaki S, Masunaga H, Shimizu N, Igarashi N, Sakurai S. Small-angle X-ray scattering studies on melting and recrystallization behaviors of poly (oxyethylene) crystallites in poly (d, l-lactide)/poly (oxyethylene) blends. Polymer (Guildf). 2014;55: 2562–9.
17. NatureWorks, LLC. Technology focus report: blends of PLA with other thermoplastics. (2007), https://www.natureworksllc.com/~/media/Files/NatureWorks/Technical-Documents/Properties-Documents/PropertiesDocument_Blends-of-Ingeo-with-other-thermoplastics_pdf.pdf.
18. Saeidlou S, Huneault MA, Li H, Park CB. Poly (lactic acid) crystallization. Progress Polym Sci. 2012;37:1657–77.
19. Li H, Huneault MA. Effect of nucleation and plasticization on the crystallization of poly (lactic acid). Polymer (Guildf). 2007;48: 6855–66.
20. Mochizuki M, Goto T, Kondo N, Takase Y, Kuroda Y, Fujita H. Effects of a polyglycerol fatty acid ester as a bio-based multifunctional additive on improvements of properties of polylactic acid. Polymer preprints, Japan. 2011;60(No. 2):5237.
21. Takagi H, Igarashi N, Mori T, Saijo S, Ohta H, Nagatani Y, et al. Upgrade of small angle X-ray scattering beamline BL-6A at the photon factory. AIP Conference Proceedings 1741, no. 1, 030018. New York: AIP Publishing; 2016.
22. Righetti MC, Gazzano M, Di Lorenzo ML, Androsch R. Enthalpy of melting of α′-and α-crystals of poly (l-lactic acid). Eur Polym J. 2015;70:215–20.
23. Schultz JM. Polymer crystallization: the development of crystalline order in thermoplastic polymers. New York: Oxford University Press; 2001.
24. Strobl GR. The physics of polymers: concepts of understanding their structures and behavior. Berlin: Springer, 1996.
25. Mochizuki M. Designing of high-performance/highly functional PLA. The state of the art on bioplastic technologies. K. Ohshima eds., Tokyo: CMC Publishing, 2014; 31–54.
26. Miyamoto Y, Fukao K, Miyaji H. "Small-angle x-ray scattering of isotactic polystyrene. Colloid Polym Sci. 1995;273(no. 1):66–75.
27. Wendorff JH, Fischer EW. Thermal density fluctuations in amorphous polymers as revealed by small angle X-ray diffraction. Kolloid Z Z Polym. 1973;251:884
28. Okamoto S, Yamamoto K, Nomura K, Hara S, Akiba I, Sakurai K, et al. Crystallization in microdomains of a block copolymer comprising semicrystalline block observed by simultaneous measurement of SAXS and WAXS with H v-SALS or DSC. J Macromol Sci Part B. 2004;43:279–96.